2D Self-Assembly of Fused Oligothiophenes: Molecular Control of Morphology

Chaoying Fu,[†] Federico Rosei,[‡] and Dmitrii F. Perepichka[†,*]

[†]Department of Chemistry and Center for Self-Assembled Chemical Structures, McGill University, 801 Sherbrooke Street West, Montréal, Québec, Canada H3A 0B8, and [‡]INRS—Énergie, Matériaux et Telecommunications, Université du Québec, Varennes, Québec, Canada J3X 1S2

ABSTRACT

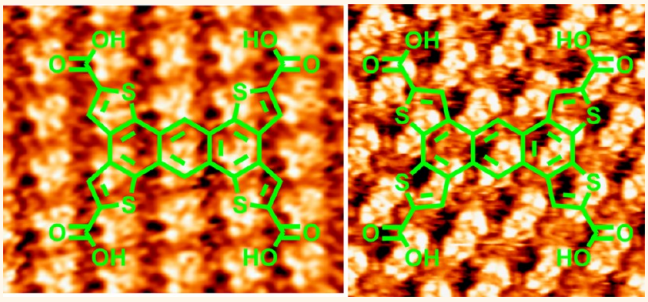

We report the synthesis and properties of two π-functional heteroaromatic tetracarboxylic acids (isomeric tetrathienoanthracene derivatives 2-TTATA and 3-TTATA) and their self-assembly on highly oriented pyrolytic graphite. Using scanning tunneling microscopy at the liquid—solid interface we show how slight geometric differences between the two isomers (position of sulfur in the molecule) lead to dramatic changes in monolayer structure. While 3-TTATA self-assembles exclusively in a highly ordered porous network *via* dimeric $R^2_2(8)$ hydrogen-bonding connection (synthon), 2-TTATA is polymorphic, forming a less ordered porous network *via* $R^2_2(8)$ synthons as well as a close-packed network *via* rare tetrameric $R^4_4(16)$ synthons. Density functional theory calculations show that the self-assembly direction is governed by the angle between the carboxylic groups and secondary interactions with sulfur atoms.

KEYWORDS: self-assembly at interfaces · oligothiophene semiconductors · hydrogen-bonded networks · scanning tunneling microscopy · polymorphism

Thiophene-based oligomers and polymers display a combination of excellent electronic properties and versatility of chemical modification, which makes them the most popular semiconducting materials in organic electronics.[1] Due to their high chemical stability and rigid molecular structure, fused ring oligothiophenes and polymers thereof have been among the prime synthetic targets in the field, leading to a number of materials showing record-breaking charge mobility in organic thin-film transistors (OTFT)[2−6] and some of the highest efficiencies in organic photovoltaic (OPV) cells.[7−9] However, the relationship between the structure of a molecule and its bulk materials properties is still not fully understood. The major challenge for predicting the performance of a given organic semiconductor is our inability to rationally control molecular packing and morphology of thin films, which ultimately determines the charge transport, recombination, and other critical device parameters.

Model studies of molecular self-assembly on surfaces by scanning tunneling microscopy (STM) allow correlating molecular structure with supramolecular organization in monolayers and ultrathin films and thus are of particular relevance for understanding molecular structure—device relationships in such materials. The self-assembly of alkylated oligothiophenes has been intensively explored, providing fundamental insights into the role of the length and position of the alkyl substituents on molecular packing controlled by van der Waals interactions.[10−16] In principle, a better control over molecular organization could be achieved by using directional interactions, such as hydrogen bonding (H-bonding). Several papers explored 2D self-assembly of oligothiophenes through H-bonding of urea,[17] peptides,[18−20] or carboxylic groups;[18,21] all of these molecules also contained alkyl chains, which favor a densely packed arrangement of molecules. On the other hand, porous supramolecular structures offer new interesting opportunities for tuning electronic properties of the films through host—guest chemistry. Toward this goal, Bäuerle *et al.* have designed a macrocyclic oligothiophene building block (with molecularly defined cavity) and using STM studied its coassembly with a C_{60} fullerene acceptor that mimics the structure of a bulk heterojunction solar cell, though restricted to two dimensions.[22] We have recently shown that porous H-bonding molecular networks can be assembled on surfaces from

* Address correspondence to dmitrii.perepichka@mcgill.ca.

Received for review June 7, 2012 and accepted August 7, 2012.

Published online August 07, 2012
10.1021/nn3025139

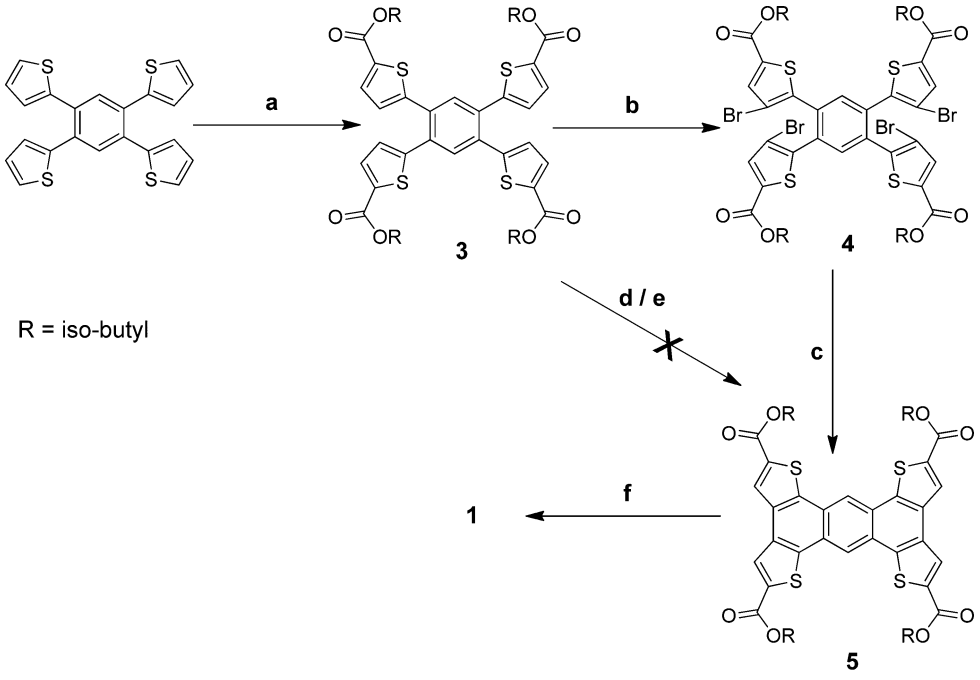

Scheme 1. Synthesis of 2-TTATA[a]

[a] (a) n-BuLi, dry THF, −78 °C; isobutyl chloroformate, −78 °C to RT; (b) Br_2, DCM, reflux; (c) $Ni(cod)_2$, bipyridine, dry DMF, 80 °C; (d) $FeCl_3$, $MeNO_2$/DCM, RT; (e) $O_2/h\nu$, toluene, RT, overnight; (f) CsOH, ethanol/water, reflux; then HCl.

terthienobenzenetricarboxylic acid (TTBTA). The resulting chickenwire network can host one, two, or three C_{60} molecules per cavity and imposes an unusual ordering effect of C_{60} dimer and trimers that was described in terms of charge-transfer interactions.[23]

In this paper, we report the synthesis of two isomeric *tetra*dentate H-bonding building blocks, **1** (2-TTATA) and **2** (3-TTATA), and study of their 2D self-assembly on the surface of highly oriented pyrolytic graphite (HOPG). These molecules were chosen because π-conjugated tetrathienoanthracene (TTA) cores of **1** and **2** have recently shown promising semiconducting properties in OTFT[24,25] and OPV[9] devices. HOPG is a suitable model surface, as it provides electrical conductivity necessary for STM imaging, yet it is chemically inert. Using STM at the solid−liquid interface and analyzing the resulting packing motifs with the aid of density functional theory (DFT) calculations, we show how subtle differences between the isomers **1** and **2** are translated in dramatically different self-assembled patterns. We demonstrate the formation of close-packed and porous networks with the geometry and chemical environment of the pores controlled by the isomeric structure of the molecular building block.

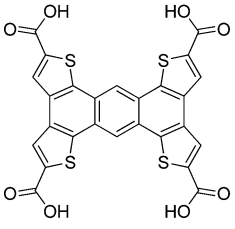

2-TTATA (1)

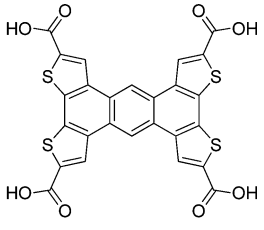

3-TTATA (2)

RESULTS

Synthesis and Electronic Structure of Building Blocks. The synthesis of 2-TTATA (Scheme 1) commenced from tetrakis(thienyl-2)benzene,[25] which was lithiated at its most reactive 2-position with *n*-BuLi and treated with isobutylchloroformate to generate tetraester **3** in 92% yield. Our attempts to directly cyclize **3**, either chemically ($FeCl_3$) or photochemically (O_2, $h\nu$) did not generate the desired product **5**. This must be due to the electron-withdrawing effect of carboxylic groups, which disfavor oxidative cyclization. To overcome this problem, the 4-position of tetraester **3** was first activated by bromination in 72% yield, and then the resulting tetrabromide **4** was subject to Yamamoto coupling using $Ni(cod)_2$ to afford fully cyclized ester **5**. The isobutyl chains were specifically chosen to induce solubility (preliminary experiments with tetraethyl ester had failed). After purification, the ester groups were cleaved off by saponification hydrolysis to afford the desired 2-TTATA, **1**. Using cesium hydroxide is important, as it creates a water-soluble TTATA salt.

The 3-TTATA (Scheme 2) building block was constructed in a similar manner yet adopting a shorter pathway. Lithiation of tetrakis(thienyl-3)benzene followed by reaction with isobutylchloroformate led to preferential substitution of the least hindered position, affording tetraester **6** with 31% purified yield. The expected higher electron density of the 2-position in **5** (as compared to the 3-position in **3**) allowed for oxidative cyclization, which was carried out with $FeCl_3$,

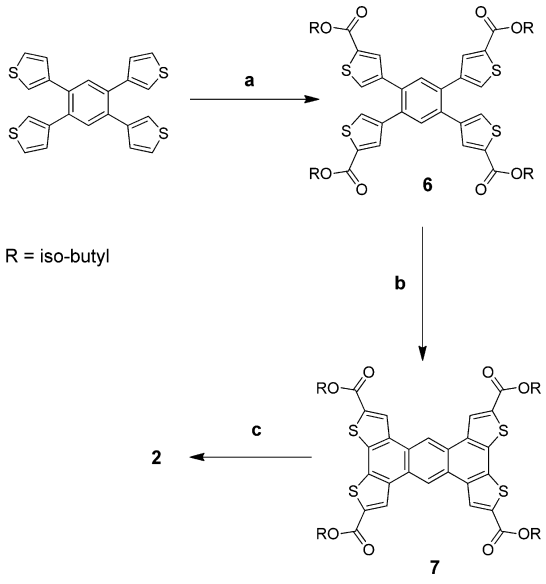

Scheme 2. Synthesis of 3-TTATA[a]

[a] (a) n-BuLi, dry THF, −78 °C; isobutyl chloroformate, −78 °C to RT; (b) $FeCl_3$, $MeNO_2$/DCM, RT; (c) CsOH, ethanol/water, reflux; then HCl.

giving tetraester **7** in 34% purified yield. Saponification of the latter afforded the desired 3-TTATA, **2**.

Due to very low solubility of tetraacids **1** and **2**, their isobutyl esters were employed to interrogate the optoelectronic properties of these building blocks. Electronic absorption spectra of both isomers 2-TTA ester **5** and 3-TTA ester **7** show several vibronically structured bands in the ~300−450 nm spectral range, characteristic for a thienoacene core (Figure 1). The longest wavelength absorption peak of **5** (438 nm) is very weak and is red-shifted vs that of **7** (412 nm, moderate intensity). The emission bands are also vibronically structured and reveal the same red shift of **5** (λ^{PL}_{max} 441 nm) vs **7** (λ^{PL}_{max} 428 nm). Comparing with the unsubstituted tetrathienoanthracenes,[25] ester groups causes a slight red shift of both absorption and emission bands (~20−30 nm), which can be attributed to extending the π-conjugation on alkoxycarbonyl substituents.

Time-dependent DFT suggests that the moderately strong longest wavelength absorption of the 3-TTATA isomer (436 nm, $f = 0.24$) is a HOMO−LUMO transition. In contrast, the HOMO−LUMO transition is symmetry forbidden for the 2-TTATA; the first allowed transition for this isomer is a mixture of HOMO−1→LUMO and HOMO→LUMO+1, and it has a very low oscillator strength (430 nm, $f = 0.01$), in agreement with the experiment. The calculated transition energies for both isomers reproduce the experimental values within 0.15 eV, but show an opposite trend for the two isomers (see also Supporting Information (SI)). This should not be particularly surprising considering that different orbitals are involved in the excitation of 2-TTA and 3-TTA isomers.

Self-Assembly of 2-TTATA. Applying a saturated solution of 2-TTATA onto HOPG leads to immediate formation of

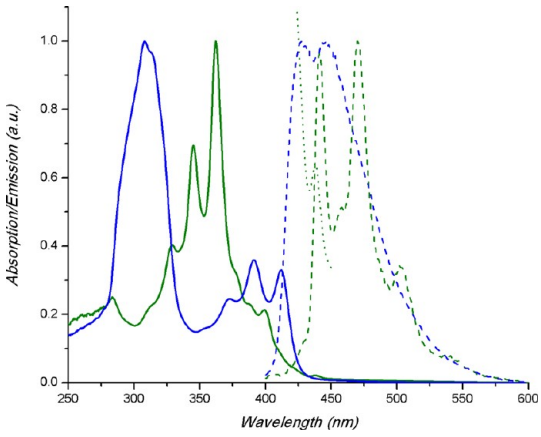

Figure 1. Absorption (solid line) and emission (dashed line) spectrum of compounds 5 (green) and 7 (blue). The dotted line is a magnification of the first absorption peak of 5.

monolayers of molecular networks as observed by STM (Figure 2). Coexistence of domains of two distinct (porous and close-packed) polymorphs was observed in the beginning of STM scanning. During the time of a typical experiment (1−2 h), the patches of porous network gradually decrease in size so that the surface is eventually covered with a large single domain of the close-packed polymorph (Figure 3).

High-resolution STM imaging of the porous network reveals an oblique unit cell (1.7 ± 0.1 nm, 1.7 ± 0.1 nm, 73 ± 2°). Each 2-TTATA molecule is resolved as a bright dumbbell, closely resembling the molecular structure. This allows identifying the orientation of each molecule with respect to its neighbors. The long-range order with parallel orientation of the molecules is preserved in the center of the domains (as highlighted by structure A and corresponding model of the molecular cluster, Figure 2). However, the rotational disorder of the molecules is frequently observed at the domain edges (structure B). Interestingly, such orientational "freedom" of the molecules allows the smooth connection of neighboring domains. Figure 2 shows that two porous domains which are rotated 84° vs each other and related by a mirror-plane symmetry, are connected *via* structure C. This phenomenon would also indicate potential frustration in growing single crystals of 2-TTATA and its derivatives.

The more frequently observed close-packed polymorph of 2-TTATA (Figure 3) exhibits a rectangular unit cell (1.6 ± 0.1 nm, 1.5 ± 0.1 nm, 88 ± 2°). The appearance of the molecules is similar albeit not identical to that in the porous network, thus emphasizing the effect of molecular packing on the density of states on the surface. Simultaneous imaging of the molecular network and HOPG surface in the same frame (and subsequent 2D-FFT analysis) and imaging of multiple domains show that one vector of the molecular unit cell is coaligned with the main symmetry axes of the HOPG lattice (SI). This suggests that molecule−substrate interaction

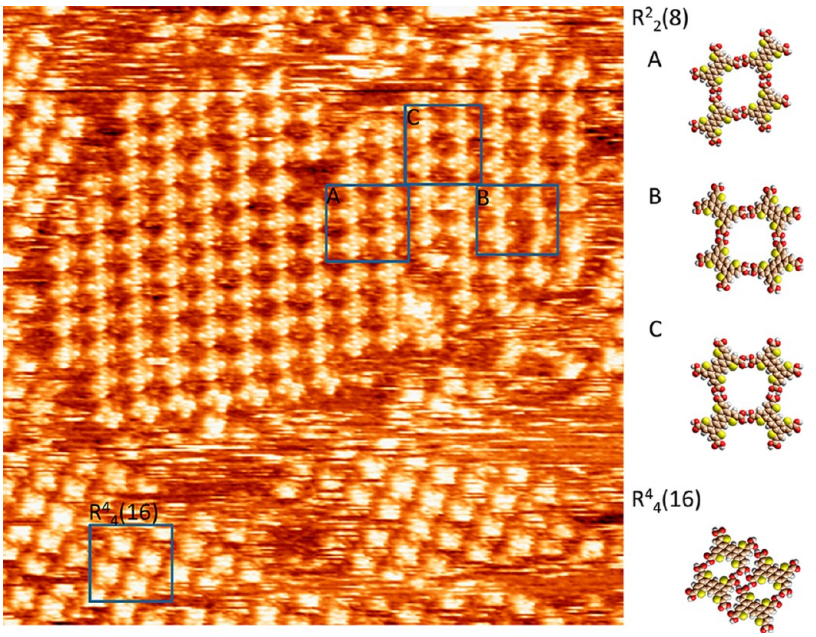

Figure 2. STM image (30 nm × 30 nm) of 2-TTATA adlayer formed at the HOPG/trichlorobenzene/octanoic acid interface. V_b = −800 mV, I_t = 0.3 nA. DFT-optimized molecular models of tetrameric molecular clusters $R^2_2(8)$ (A, B, C) and $R^4_4(16)$, corresponding to molecular arrangements in highlighted areas of the image, are shown on the right.

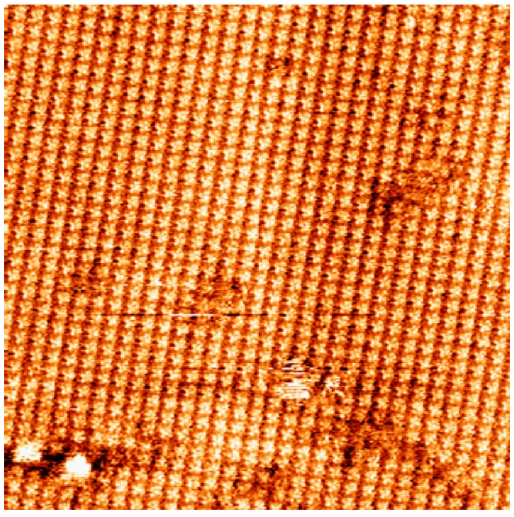

Figure 3. STM image (50 nm × 50 nm) of a single domain of the 2-TTATA close-packed structure formed at the HOPG/trichlorobenzene/octanoic acid interface. V_b = −800 mV, I_t = 0.3 nA.

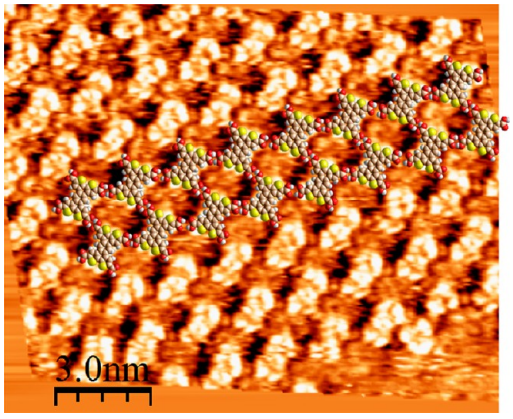

Figure 4. STM image (15 nm × 15 nm) of a molecular network formed by 3-TTATA on HOPG (V_b = −750 mV, I_t = 0.25 nA).

plays a significant role in the overall thermodynamic stability of the close-packed polymorph.

Self-Assembly of 3-TTATA. In all of our experiments, the self-assembly of 3-TTATA at the liquid−solid interface forms only a porous molecular network with an oblique unit cell (1.6 ± 0.1 nm, 1.7 ± 0.1 nm, 75 ± 2°) (Figure 4). Similar to 2-TTATA, one unit cell vector (b = 1.68 nm) is coaligned with one of the main symmetry axes of HOPG (SI). Each 3-TTATA molecule is well resolved into a rectangle on the STM images. The elongated appearance of these molecules comparing to 2-TTATA reflects the altered position of sulfur atoms, which contributes significantly to the STM contrast. Unlike 2-TTATA, the molecules of 3-TTATA are well ordered in the oblique structure, with no rotational defects of the kind shown in Figure 2.

DISCUSSION

Carboxylic acids are H-bonding building blocks with highly directional binding and predictable self-assembly.[26] They most often associate *via* dimeric H-bonding ring synthon $R^2_2(8)$. The binding *via* trimeric $R^3_3(12)$, tetrameric $R^4_4(16)$, and seximeric $R^6_6(24)$ synthons are also known but extremely rare.[27]

The majority of the so far reported H-bonding molecular networks have been created with di- and tricarboxylic acids, and just a few papers reported the surface self-assembly of tetracarboxylic building blocks.[28−34]

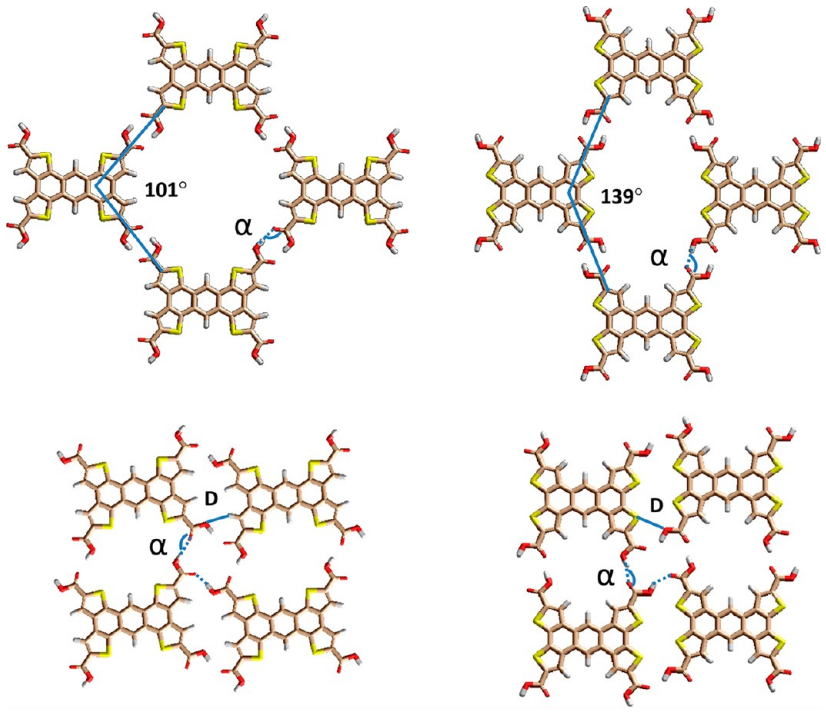

Figure 5. DFT-PBC models of 2-TTATA (left) and 3-TTATA (right) in porous (top) and close-packed (bottom) networks. α denotes the angle of the C═O···H bond in the $R^2_2(8)$ synthon and $R^4_4(16)$ synthon. D denotes the secondary short contacts: O···H (2.5 Å) for 2-TTATA and S···O (3.1 Å) for 3-TTATA.

In all studied examples, the angle α between the carboxylic groups, which controls the geometry of the resulting pattern, was either 90°, 120°, or 180°. In the TTATA isomers studied here, the angle between the carboxylic group depends on the orientation of the thiophene ring in the polycyclic structure and is equal to 101° for 2-TTATA and 139° for 3-TTATA (Figure 5). Accordingly, a kagome pattern, commonly observed for tetradentate building blocks with α = 120°,[32] is unfavorable for TTATA derivatives, and their $R^2_2(8)$ H-bonding leads exclusively to oblique structures.

For the 2-TTATA isomer, the angle between the four binding sites (101°/79°) is sufficiently close to that of C_4 symmetric building blocks (90°), leading to partial orientational disorder of this molecule in the oblique unit cell (structures B and C, Figure 2). This assumption is supported by DFT calculations of tetrameric clusters of 2-TTATA bonded *via* the $R^2_2(8)$ synthon (SI). The calculated binding energy of cluster A representing the oblique unit cell (10.04 kcal/mol per H-bond) is only marginally larger than that in clusters C (10.01 kcal/mol) and B (9.85 kcal/mol) with two and one "misoriented" molecules, respectively. Such tolerance of a 2-TTATA porous network toward orientational disorder allows connecting an adjacent crystalline domain without disruption of H-bonding, which minimizes the occurrence of Ostwald ripening.[35] At the same time, the enthalpic differences associated with inclusion of clusters B and C within the ordered phase are apparently large enough to prevent a complete entropy-driven randomization. A similar phenomenon involving transitions between the ordered and disordered 2D phases of other tetracarboxylic acids has been recently studied in detail by Beton *et al.*[34]

TABLE 1. Comparison of 2-TTATA and 3-TTATA Polymorphs by Molecular Modeling[a]

	unit cell parameters				
network	α/nm	β/nm	γ/°	packing density (molecule/nm²)	binding energy (kcal/mol/H-bond)
2-TTATA close-packed	1.50	1.27	89.6	0.52	9.2
2-TTATA porous	1.72	1.72	80.5	0.34	10.0
3-TTATA close-packed	1.40	1.36	85.3	0.52	8.0
3-TTATA porous	1.65	1.65	79.8	0.4	10.0

[a] PBC-DFT calculation at the B3LYP/6-31G(d) level.

For 3-TTATA, the angles between the binding sites (139° and 41°) establish unambiguously C_2 binding symmetry. Accordingly, the modeling (SI) shows that the only tetrameric cluster capable of providing four $R^2_2(8)$ connections between the molecules is that represented by the oblique unit cell shown in Figure 5 (binding energy 10.03 kcal/mol).

To shed further light on the self-assembly of the new tetradentate building blocks, we have performed DFT calculations in periodic boundary conditions (PBC) for 2D crystals of both TTATA isomers, in both porous and close-packed polymorphs (Table 1). For porous networks, practically the same H-bonding energy was found for 2-TTATA and 3-TTATA (10.0 kcal/mol), ruling out long-range electronic effects of heteroatoms on self-assembly.

Close-packed polymorphs of both molecules, which can be formed *via* $R^4_4(16)$ H-bonding synthons, reveal lower stabilization energies for 2-TTATA (9.2 kcal/mol) and particularly for 3-TTATA (8.0 kcal/mol). This can be explained by a less favorable angle of the C═O···H bond[23,26] in $R^4_4(16)$ (140−160°, Figure 5) compared with that of the $R^2_2(8)$ synthon (125°). Indeed, $R^4_4(16)$ is a very rare H-bonding synthon, with only two previous observations in 2D molecular self-assembly.[29,36] On the other hand, the association of tetracarboxylic acids *via* this synthon leads to a significantly increased packing density, from 0.34 molecule/nm^2 for a porous polymorph of 2-TTATA to 0.52 molecule/nm^2 for its close-packed structure (Figure 5). The increased amount of molecular network−substrate interactions counteracts the decrease of intermolecular binding energy. Accordingly, for 2-TTATA both polymorphs have been observed.

Another factor that disfavors $R^4_4(16)$ H-bonding is the increased steric repulsion between the aromatic cores of neighboring molecules. The substantially lower energy of 3-TTATA binding *via* the $R^4_4(16)$ synthon (8.0 kcal/mol) could be attributed to repulsive S···O interactions (3.1 Å; *cf.* the sum of van der Waals radii of S and O, 3.3 Å) (Figure 5). Such decrease of the binding energy is not compensated by a relatively small increase of the packing density (from 0.4 to 0.52 molecule/nm^2), and the close-packed polymorph of 3-TTATA was never observed.

CONCLUSIONS

We have reported the synthesis, molecular properties, and STM investigation of self-assembly of two new isomeric fused oligothiophenes. A detailed analysis of STM images and DFT calculations reveal that different self-assembly behavior of the two isomers can be rationalized *via* different angles of connections imposed by the asymmetric thiophene ring, together with the effect of secondary weak interactions of sulfur atoms. Under our conditions 3-TTATA produces only one stable polymorph (oblique porous structure) in large domains. However, the frustrated symmetry of 2-TTATA leads to ambiguity of its 2D crystallization behavior and gives rise to an assembly of several porous $R^2_2(8)$- and close-packed $R^4_4(16)$-based self-assembly motifs. Noteworthy, the 2-TTATA molecule is among the very few molecular building block examples that employ $R^4_4(16)$ H-bonding synthons.

We note that the difference of self-assembly behavior of 2-TTATA and 3-TTATA was also echoed in the earlier observed (but not completely understood) effect of the position of sulfur on field-effect mobility measured in thin films of other substituted tetrathienoanthracene isomers.[25] The demonstrated control of self-assembly *via* tweaking the fine structure of the building block opens opportunities for designing complex supramolecular semiconducting materials.

METHODS

Graphite of grade SPI-2 from SPI Supplies was freshly cleaved by adhesive tape before every experiment. Octanoic acid (98%) and 1,2,4-trichlorobenzene were purchased from Sigma-Aldrich and used without further purification. STM images were acquired either from NanoSurf EasyScan 2 or Digital Instruments Inc. (Veeco) NanoScope IIIa. The 80/20 Pt/Ir STM tips were mechanically cut with a wire cutter. Molecular monolayers were prepared by applying a drop of the TTATA in a 1:1 octanoic acid/1,2,4-trichlorobenzene mixture on graphite surface. The nominal concentration of the suspension mixture was *ca.* 0.005 M. All the raw images were processed from WSxM5.0[37] and SPIP 4.5.5 software. The periodicities of the close-packed network of 2-TTATA and open network of 3-TTATA were calibrated using the underlying graphite lattice unit cell through 2D-FFT. The periodicity of the porous structure of the 2-TTATA open network was calibrated by that of the close-packed structure in the same scanning frame. DFT calculations were performed using the Gaussian 3.0W[38] software.

Tetraisobutyl 5,5′,5″,5‴-(Benzene-1,2,4,5-tetrayl)tetrakis(thiophene-2-carboxylate) (3). A solution of 1,2,4,5-tetra(thiophen-2-yl)-benzene[25] (0.42 g, 1.0 mmol) in THF (20 mL) was stirred at −78 °C in a N_2 atmosphere; then *n*-butyllithium (4.0 mL, 1.7 M in hexane, 6.8 mmol) was added dropwise. The reaction mixture was allowed to warm to room temperature during 3 h, and it precipitated after being stirred another 1 h. When the reaction mixture was cooled to −78 °C, isobutyl chloroformate (1.0 mL, 7.6 mmol) was added, and white precipitates dissolved immediately. The clear orange reaction mixture was stirred and warmed to room temperature gradually overnight. It was extracted with ethyl acetate and washed with water. The organic phase was separated and dried over magnesium sulfate, and the solvent was evaporated, affording **1** as a yellow solid (0.76 g, 92%). Mp: 102−103 °C. ^{1}H NMR (δ, $CDCl_3$): 7.67 (2H, s), 7.66 (4H, d, J = 4.0 Hz), 6.91 (4H, d, J = 4.0 Hz), 4.07 (8H, d, J = 6.6 Hz), 2.05 (4H, m), 0.99 (24H, d, J = 6.8 Hz). ^{13}C NMR (δ, $CDCl_3$): 161.97, 147.03, 134.83, 133.57, 133.32, 128.49, 71.25, 27.86, 19.09. MS (MALDI): *m/z* 829.39 [M + Na].

Tetraisobutyl 5,5′,5″,5‴-(Benzene-1,2,4,5-tetrayl)tetrakis(4-bromothiophene-2-carboxylate) (4). A solution of **3** (1.10 g, 1.36 mmol) in DCM (12 mL) was stirred under N_2 flow while bromine (0.4 mL, 8 mmol) was added dropwise. The reaction mixture went from orange to green-blue. After being stirred at room temperature for 12 h, bromine (0.2 mL, 7.8 mmol) was added at room temperature and the reaction mixture was refluxed for another 12 h. Na_2SO_3 solution (10%) was added to the cooled dark mixture, and the organic phase was extracted, washed with $NaHCO_3$, and dried over magnesium sulfate. The solvent was removed, and the crude product was dissolved in dichloromethane and passed through silica gel. Recrystallization from hexane/dichloromethane afforded **2** as a white solid (1.10 g, 72%). Mp: 168−171 °C. ^{1}H NMR (δ, $CDCl_3$): 7.76 (2H, s), 7.64 (4H, s), 4.05 (8H, d, J = 6.6 Hz), 2.03 (4H, m), 0.98 (24H, d, J = 6.6 Hz). ^{13}C NMR (δ, $CDCl_3$): 160.95, 141.11, 135.69, 135.37, 135.02, 133.13, 112.17, 71.62, 27.80, 19.05. MS (MALDI): *m/z* 1144.99 [M + Na].

Tetraisobutyl Anthra[1,2-*b*:4,3-*b*′:5,6-*b*″:8,7-*b*‴]tetrathiophene-2,5,9,12-tetracarboxylate (5). A solution of Ni(cod)$_2$ (0.27 g, 0.99 mmol) and compound **4** (0.25 g, 0.23 mmol) in dry dimethylformamide (5 mL) was stirred in a Schlenk tube at room temperature, while 1,5-cyclooctadiene (0.13 mL, 1.06 mmol) was added. The reaction mixture was deoxygenated by three freeze−pump−thaw cycles followed by adding 2,2′-bipyridine (0.15 g, 0.96 mmol) under N_2 flow. The reaction mixture was then sealed and stirred at 80 °C for 2 days, during which it turned from a purple solution to a black suspension. The reaction mixture was cooled to room temperature, water was added, and the organic phase was

extracted with chloroform and dried over magnesium sulfate. The solvent was removed, affording a crude product as a brown-orange solid (0.12 g, 67%). The compound showed a tendency to stack on silica (either crystallization or hydrolysis), and purification was achieved by recrystallization from chloroform to yield pure **3** (0.02 g, 11%). Mp: >210 °C (dec). ^{1}H NMR (δ, $CDCl_3$): 8.84 (2H, s), 8.38 (4H, s), 4.23 (8H, d, J = 6.4 Hz), 2.20 (4H, m), 1.13 (24 H, d, J = 6.8 Hz). MS (MALDI): m/z 802.64 [M^+].

Anthra[1,2-*b*:4,3-*b*′:5,6-*b*″:8,7-*b*‴]tetrathiophene-2,5,9,12-tetracarboxylic Acid (1). Tetraester **5** (0.026 g, 0.032 mmol) and cesium hydroxide (50 wt % solution in water, 5 mL) were refluxed in ethanol (75 mL) overnight with pH > 11. The resulting solution was acidified by hydrochloric acid to pH < 1, and the formed precipitate was filtered off and washed with chloroform. Mp: (dec >300 °C). ^{1}H NMR (δ, DMSO-d_6): 9.54 (2H, s), 9.24 (4H, s), MS (MALDI): m/z 577.75 [M^+]. HRMS (ESI−): m/z calcd for [$C_{26}H_9O_8S_4$] 576.9186, found 576.9199.

Tetraisobutyl 4,4′,4″,4‴-(Benzene-1,2,4,5-tetrayl)tetrakis(thiophene-2-carboxylate) (6). A solution of 1,2,4,5-tetra(thiophen-3-yl)-benzene[25] (0.50 g, 1.23 mmol) in dry THF (24 mL) was stirred at −78 °C under N_2 flow while *tert*-butyllithium (5.35 mL, 1.7 M in hexane, 9.10 mmol) was added dropwise. The reaction mixture was allowed to warm and stirred at room temperature for 1 h, leading to formation of a white precipitate. The reaction mixture was cooled to −78 °C, isobutyl chloroformate (1.5 mL, 11 mmol) was added, and the precipitate dissolved immediately. The clear yellow reaction mixture was stirred and allowed to warm to room temperature overnight. It was extracted with ethyl acetate and washed with water. The organic phase was separated and dried over magnesium sulfate, and the solvent was evaporated, affording an orange-yellow, oily product. Trituration of the crude product with hexane yielded **5** as a white solid (0.31 g, 31%). Mp: 166−168 °C. ^{1}H NMR (δ, $CDCl_3$): 7.58 (4H, d, J = 1.6 Hz), 7.52 (2H, s), 7.28 (2H, d, J = 1.6 Hz), 4.05(8H, d, J = 6.6 Hz), 2.03 (4H, m, J = 6.8 Hz), 0.98 (24H, d, J = 6.6 Hz). ^{13}C NMR (δ, $CDCl_3$): 161.94, 141.03, 134.29, 134.08, 134.04, 131.77, 130.17, 71.20, 27.84, 19.07. MS (MALDI): m/z 898.93 [M + Na].

Tetraisobutyl Anthra[2,1-*b*:3,4-*b*′:6,5-*b*″:7,8-*b*‴]tetrathiophene-2,5,9,12-tetracarboxylate (7). A solution of **6** (0.29 g, 0.37 mmol) in dry DCM (18 mL) was stirred while a solution of dry iron(III) chloride (0.25 g, 1.54 mmol) in nitromethane (6 mL) was added. Methanol (150 mL) was added after the product was kept running overnight, and the reddish-brown reaction mixture precipitated after 1 h. The precipitate was filtrered and rinsed with water (0.99 g, 34%), afforing pure product **6** as an orange-yellow solid. Mp: >209 °C (dec). ^{1}H NMR (δ, $CDCl_3$): 9.06 (2H, s), 8.73 (4H, s), 4.25 (8H, d, J = 6.8 Hz), 2.24 (4H, m), 1.14 (24H, J = 7.2 Hz). MS (APCI+): m/z 802.18 [M^+].

Anthra[2,1-*b*:3,4-*b*′:6,5-*b*″:7,8-*b*‴]tetrathiophene-2,5,9,12-tetracarboxylic Acid (2). Tetraester **7** (0.005 g, 0.006 mmol) and cesium hydroxide (50 wt % solution in water, 1 mL) were refluxed in ethanol (25 mL) overnight at pH > 11. The resulting solution was acidified by hydrochloric acid to pH < 1, and the formed precipitate was filtered off and washed with water and chloroform. Mp: >300 °C (dec). ^{1}H NMR (δ, DMSO-d_6): 9.82 (2H, s), 9.41 (4H, s). MS (MALDI): m/z 577.77 [M^+]. HRMS (ESI−): m/z calcd for [$C_{26}H_9O_8S_4$] 576.9186, found 576.9198.

Conflict of Interest: The authors declare no competing financial interest.

Supporting Information Available: Calculation details; additional STM images of the molecular networks; NMR and MS spectra of the new compounds. This material is available free of charge *via* the Internet at http://pubs.acs.org.

Acknowledgment. This work was supported by NSERC of Canada (Discovery and RTI grants) and a FQRNT Team Grant.

REFERENCES AND NOTES

1. Perepichka, I. F.; Perepichka, D. F.; Meng, H. In *Handbook of Thiophene-Based Materials: Applications in Electronics and Photonics*, Vol. 2; Perepichka, I. F.; Perepichka, D. F., Eds.; Wiley VCH, 2009.
2. McCulloch, I.; Heeney, M.; Bailey, C.; Genevicius, K.; Macdonald, I.; Shkunov, M.; Sparrowe, D.; Tierney, S.; Wagner, R.; Zhang, W.; Chabinyc, M. L.; *et al*. Liquid-Crystalline Semiconducting Polymers with High Charge-Carrier Mobility. *Nat. Mater.* **2006**, *5*, 328–333.
3. Rieger, R.; Beckmann, D.; Pisula, W.; Steffen, W.; Kastler, M.; Mullen, K. Rational Optimization of Benzo[2,1-*b*;3,4-*b*′]-dithiophene-Containing Polymers for Organic Field-Effect Transistors. *Adv. Mater.* **2010**, *22*, 83–86.
4. Kang, M. J.; Doi, I.; Mori, H.; Miyazaki, E.; Takimiya, K.; Ikeda, M.; Kuwabara, H. Alkylated Dinaphtho[2,3-*b*:2′,3′-*f*]thieno-[3,2-*b*]thiophenes (*Cn*-DNTTs): Organic Semiconductors for High-Performance Thin-Film Transistors. *Adv. Mater.* **2011**, *23*, 1222–1225.
5. Sokolov, A. N.; Atahan-Evrenk, S.; Mondal, R.; Akkerman, H. B.; Sanchez-Carrera, R. S.; Granados-Focil, S.; Schrier, J.; Mannsfeld, S. C. B.; Zoombelt, A. P.; Bao, Z. N.; *et al*. From Computational Discovery to Experimental Characterization of a High Hole Mobility Organic Crystal. *Nat. Commun.* **2011**, *2*, 437–444.
6. Schroeder, B. C.; Nielsen, C. B.; Kim, Y. J.; Smith, J.; Huang, Z. G.; Durrant, J.; Watkins, S. E.; Song, K.; Anthopoulos, T. D.; McCulloch, I. Benzotrithiophene Co-polymers with High Charge Carrier Mobilities in Field-Effect Transistors. *Chem. Mater.* **2011**, *23*, 4025–4031.
7. Chen, H. Y.; Hou, J. H.; Zhang, S. Q.; Liang, Y. Y.; Yang, G. W.; Yang, Y.; Yu, L. P.; Wu, Y.; Li, G. Polymer Solar Cells with Enhanced Open-Circuit Voltage and Efficiency. *Nat. Photonics* **2009**, *3*, 649–653.
8. Hou, J. H.; Chen, H. Y.; Zhang, S. Q.; Chen, R. I.; Yang, Y.; Wu, Y.; Li, G. Synthesis of a Low Band Gap Polymer and Its Application in Highly Efficient Polymer Solar Cells. *J. Am. Chem. Soc.* **2009**, *131*, 15586–15587.
9. He, F.; Wang, W.; Chen, W.; Xu, T.; Darling, S. B.; Strzalka, J.; Liu, Y.; Yu, L. P. Tetrathienoanthracene-Based Copolymers for Efficient Solar Cells. *J. Am. Chem. Soc.* **2011**, *133*, 3284–3287.
10. Stabel, A.; Rabe, J. P. Scanning-Tunneling-Microscopy of Alkylated Oligothiophenes at Interfaces with Graphite. *Synth. Met.* **1994**, *67*, 47–53.
11. Bäuerle, P.; Fischer, T.; Bidlingmeier, B.; Stabel, A.; Rabe, J. P. Oligothiophenes - Yet Longer - Synthesis, Characterization, and Scanning unneling Microscopy Images of Homologous, Isomerically Pure Oligo(alkylthiophene)s. *Angew. Chem., Int. Ed. Engl.* **1995**, *34*, 303–307.
12. Mena-Osteritz, E. Superstructures of Self-Organizing Thiophenes. *Adv. Mater.* **2002**, *14*, 609–616.
13. Bonini, M.; Zalewski, L.; Breiner, T.; Dotz, F.; Kastler, M.; Schadler, V.; Surin, M.; Lazzaroni, R.; Samori, P. Competitive Physisorption among Alkyl-substituted π-Conjugated Oligomers at the Solid-Liquid Interface: Towards Prediction of Self-Assembly at Surfaces from a Multicomponent Solution. *Small* **2009**, *5*, 1521–1526.
14. Yang, Z. Y.; Zhang, H. M.; Yan, C. J.; Li, S. S.; Yan, H. J.; Song, W. G.; Wan, L. J. Scanning Tunneling Microscopy of the Formation, Transformation, and Property of Oligothiophene Self-organizations on Graphite and Gold Surfaces. *Proc. Natl. Acad. Sci. U. S. A.* **2007**, *104*, 3707–3712.
15. Yang, Z. Y.; Zhang, H. M.; Pan, G. B.; Wan, L. J. Effect of the Bridge Alkylene Chain on Adlayer Structure and Property of Functional Oligothiophenes Studied with Scanning Tunneling Microscopy and Spectroscopy. *ACS Nano* **2008**, *2*, 743–749.
16. Tongol, B. J. V.; Wang, L.; Yau, S. L.; Otsubo, T.; Itaya, K. Nanostructures and Molecular Assembly of β-Blocked Long Oligothiophenes up to the 96-Mer on Au(111) as Probed by *in Situ* Electrochemical Scanning Tunneling Microscopy. *J. Phys. Chem. C* **2009**, *113*, 13819–3824.
17. De Feyter, S.; Larsson, M.; Gesquiere, A.; Verheyen, H.; Louwet, F.; Groenendaal, B.; van Esch, J.; Feringa, B. L.; De Schryver, F. Unusual Two-Dimensional Multicomponent Self-Assembly Probed by Scanning Tunneling Microscopy. *ChemPhysChem* **2002**, *3*, 966–969.
18. Klok, H. A.; Rosler, A.; Gotz, G.; Mena-Osteritz, E.; Bäuerle, P. Synthesis of a Silk-Inspired Peptide Oligothiophene Conjugate. *Org. Biomol. Chem.* **2004**, *2*, 3541–3544.
19. Schillinger, E.-K.; Mena-Osteritz, E.; Hentschel, J.; Börner, H.; Bäuerle, P. Oligothiophene *versus* β-Sheet Peptide: Synthesis

and Self-Assembly of an Organic Semiconductor Peptide Hybrid. *Adv. Mater.* **2009**, *21*, 1562–1567.
20. Shaytan, A. K.; Schillinger, E. K.; Khalatur, P. G.; Mena-Osteritz, E.; Hentschel, J.; Borner, H. G.; Bäuerle, P.; Khokhlov, A. R. Self-Assembling Nanofibers from Thiophene-Peptide Diblock Oligomers: A Combined Experimental and Computer Simulations Study. *ACS Nano* **2011**, *5*, 6894–6909.
21. Gong, J. R.; Wan, L. J.; Jiu, T. G.; Li, Y. L.; Zhu, D. B.; Deng, K. Molecular Architecture of Oligothiophene on a Highly Oriented Pyrolytic Graphite Surface by Employing Hydrogen Bondings. *J. Phys. Chem. B* **2006**, *110*, 17043–17049.
22. Kromer, J.; Rios-Carreras, I.; Fuhrmann, G.; Musch, C.; Wunderlin, M.; Debaerdemaeker, T.; Mena-Osteritz, E.; Bäuerle, P. Synthesis of the First Fully α-Conjugated Macrocyclic Oligothiophenes: Cyclo[*n*]thiophenes with Tunable Cavities in the Nanometer Regime. *Angew. Chem., Int. Ed.* **2000**, *39*, 3481–3486.
23. MacLeod, J. M.; Ivasenko, O.; Fu, C. Y.; Taerum, T.; Rosei, F.; Perepichka, D. F. Supramolecular Ordering in Oligothiophene-Fullerene Monolayers. *J. Am. Chem. Soc.* **2009**, *131*, 16844–16850.
24. Liu, W. J.; Zhou, Y.; Ma, Y. G.; Cao, Y.; Wang, J.; Pei, J. Thin Film Organic Transistors from Air-Stable Heteroarenes: Anthra[1,2-*b*:4,3-*b*′:5,6-*b*″:8,7-*b*‴]tetrathiophene Derivatives. *Org. Lett.* **2007**, *9*, 4187–4190.
25. Brusso, J. L.; Hirst, O. D.; Dadvand, A.; Ganesan, S.; Cicoira, F.; Robertson, C. M.; Oakley, R. T.; Rosei, F.; Perepichka, D. F. Two-Dimensional Structural Motif in Thienoacene Semiconductors: Synthesis, Structure, and Properties of Tetrathienoanthracene Isomers. *Chem. Mater.* **2008**, *20*, 2484–2494.
26. Ivasenko, O.; Perepichka, D. F. Mastering Fundamentals of Supramolecular Design with Carboxylic Acids. Common Lessons from X-ray Crystallography and Scanning Tunneling Microscopy. *Chem. Soc. Rev.* **2011**, *40*, 191–206.
27. The notion $R^x_y(Z)$ describes a ring synthon with *x* H-bond donors, *y* H-bond acceptors, and Z total atoms in the ring.
28. Yoshimoto, S.; Yokoo, N.; Fukuda, T.; Kobayashi, N.; Itaya, K. Formation of Highly Ordered Porphyrin Adlayers Induced by Electrochemical Potential Modulation. *Chem. Commun.* **2006**, 500–502.
29. Lei, S. B.; Wang, C.; Yin, S. X.; Wang, H. N.; Xi, F.; Liu, H. W.; Xu, B.; Wan, L. J.; Bai, C. L. Surface Stabilized Porphyrin and Phthalocyanine Two-Dimensional Network Connected by Hydrogen Bonds. *J. Phys. Chem. B* **2001**, *105*, 10838–10841.
30. Zhou, H.; Dang, H.; Yi, J. H.; Nanci, A.; Rochefort, A.; Wuest, J. D. Frustrated 2D Molecular Crystallization. *J. Am. Chem. Soc.* **2007**, *129*, 13774–13775.
31. Blunt, M. O.; Russell, J. C.; Gimenez-Lopez, M. D.; Garrahan, J. P.; Lin, X.; Schroder, M.; Champness, N. R.; Beton, P. H. Random Tiling and Topological Defects in a Two-Dimensional Molecular Network. *Science* **2008**, *322*, 1077–1081.
32. Blunt, M.; Lin, X.; Gimenez-Lopez, M. D.; Schroder, M.; Champness, N. R.; Beton, P. H. Directing Two-Dimensional Molecular Crystallization Using Guest Templates. *Chem. Commun.* **2008**, 2304–2306.
33. Ciesielski, A.; Samori, P. Supramolecular Assembly/Reassembly Processes: Molecular Motors and Dynamers Operating at Surfaces. *Nanoscale* **2011**, *3*, 1397–1410.
34. Stannard, A.; Russell, J. C.; Blunt, M. O.; Salesiotis, C.; Gimenez-Lopez, M. D.; Taleb, N.; Schroder, M.; Champness, N. R.; Garrahan, J. P.; Beton, P. H. Broken Symmetry and the Variation of Critical Properties in the Phase Behaviour of Supramolecular Rhombus Tilings. *Nat. Chem.* **2012**, *4*, 112–117.
35. Stabel, A.; Heinz, R.; Deschryver, F. C.; Rabe, J. P. Ostwald Ripening of Two-Dimensional Crystals at the Solid-Liquid Interface. *J. Phys. Chem.* **1995**, *99*, 505–507.
36. Xiao, W. D.; Jiang, Y. H.; Ait-Mansour, K.; Ruffieux, P.; Gao, H. J.; Fasel, R. Chiral Biphenyldicarboxylic Acid Networks Stabilized by Hydrogen Bonding. *J. Phys. Chem. C* **2010**, *114*, 6646–6649.
37. Horcas, I.; Fernandez, R.; Gomez-Rodriguez, J. M.; Colchero, J.; Gomez-Herrero, J.; Baro, A. M. WSxM: A Software for Scanning Probe Microscopy and a Tool for Nanotechnology. *Rev. Sci. Instrum.* **2007**, *78*, 013705(1—8).
38. Frisch, M. J.; Trucks, G. W.; Schlegel, H. B.; Scuseria, G. E.; Robb, M. A.; Cheeseman, J. R.; Montgomery, J. A., Jr.; Vreven, T.; Kudin, K. N.; Burant, J. C.; et al. *Gaussian 03*, Revision D.01; Gaussian, Inc.: Wallingford, CT, 2004.